

EPR and Optical Absorption Studies of VO²⁺ Doped KH₂PO₄ and KH₃C₄O₈·2H₂O Single Crystals

Recep Bıyık and Recep Tapramaz

Öndokuz Mayıs University, Faculty of Art and Sciences, Department of Physics, 55139-Samsun, Turkey

Reprint requests to Dr. R. B.; E-mail: rbiyik@omu.edu.tr

Z. Naturforsch. **61a**, 171 – 179 (2006); received December 20, 2005

VO²⁺ doped potassium dihydrogen phosphate (KH₂PO₄) and potassium tetraoxalate (KH₃C₄O₈·2H₂O) single crystals and powders are examined by electron paramagnetic resonance and optical absorption spectroscopy. Angular variations of KH₂PO₄ and KH₃C₄O₈·2H₂O single crystals show four and two different VO²⁺ sites, respectively. The local symmetry of VO²⁺ complexes is nearly axial for both host crystals. The optical absorption spectra show three bands. Spin Hamiltonian parameters are measured and molecular orbital coefficients are calculated by correlating EPR and optical absorption data for the central vanadyl ion.

Key words: EPR; Potassium Dihydrogen Phosphate; Potassium Tetraoxalate; Absorption Spectrum; Vanadyl Ion.

1. Introduction

Paramagnetic VO²⁺ ions are frequently used as probe in crystalline host materials, reflecting the local symmetry and the structural properties. Therefore the EPR spectra of VO²⁺ in different diamagnetic host lattices have been studied by many workers to get information about the structure, dynamics and environment of the host lattices [1 – 11].

Potassium dihydrogen phosphate, KH₂PO₄ (KDP), and crystals derived from it are a well-known crystal group of significant scientific and technological interest. The crystals of the family show nonlinear electromechanical behavior for acoustic applications [12]. They also show an electro optical effect, that is the refractive index changes nonlinearly with applied voltage. This nonlinear optical property of the KDP family is utilized in optics, especially for laser applications to convert the frequency of a coherent radiation to a different one and to mix different frequencies (Pockels effect). They have a very high optical damage threshold, and this can be exploited in intense laser beam applications [13, 14]. Very large and highly perfect KDP single crystals (60 cm or more cm wide) can be grown [15]. KDP undergoes a paraelectric phase transition at 122 K, where the symmetry changes from tetragonal to orthorhombic.

Because of its wide applications in technology, impurities in KDP crystals, including divalent and trivalent metal ions, are introduced and investigated to see the effects on optical, electrical and other physical properties, and also the effects on the crystal growing mechanism and face morphology [16 – 21]. Divalent and trivalent metal ions occupy different locations. Trivalent metal ions are generally adsorbed on the surface, but in a specific study it has been seen that trivalent Fe³⁺ ions occupy the FeO²⁻ site in the form of FeO₄²⁻ by compensating the charge deficiency by a nearby potassium or hydrogen vacancy [19]. Dyes are also introduced into KDP to see the effects on optical properties, growth mechanism and face morphology [22, 23].

Solutions of potassium oxalate and potassium tetraoxalate (KTO) are used for pH measurements. KTO is important because the contribution of hydroxide ions to the ionic strength is very significant. Furthermore KTO is used in photographic solutions for better development, in laundry blues, in polishers, in various cleaning powders and scouring products [24 – 26].

In this work we report X-band EPR and optical absorption spectral studies on VO²⁺ doped KDP and KTO single crystals at room temperature. The principal hyperfine coupling and g tensor components are

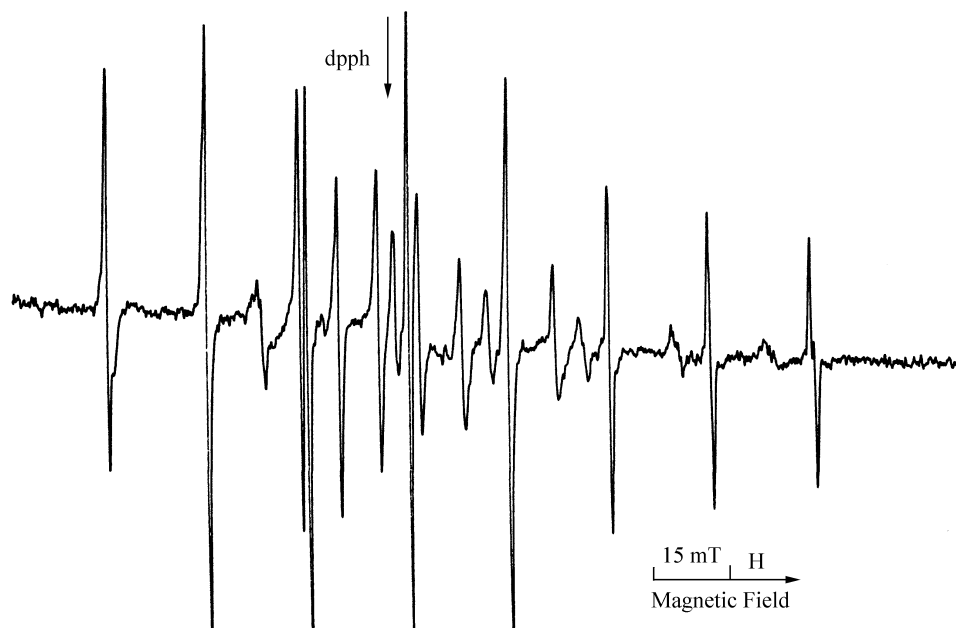


Fig. 1. EPR spectrum of VO²⁺ doped KDP single crystal with the magnetic field inclined by 5° relative to the *a* axis.

evaluated from EPR spectra, and the molecular orbital parameters of central VO²⁺ ions are evaluated using these values together with the optical absorption data.

2. Experimental

2.1. VO²⁺ Doped KDP

KDP was obtained commercially. A near-saturated aqueous solution was prepared, and 1% of VOSO₄ was added to it. The solution was left for slow evaporation. Well-developed single crystals of suitable sizes were obtained after several days. The crystals had tetragonal symmetry ($\bar{4}2m$) at room temperature with the unit cell parameters $a = 7.4529 \text{ \AA}$ and $c = 6.9751 \text{ \AA}$. The unit cell contained 4 formula units [15, 17].

2.2. VO²⁺ Doped KTO

KTO was obtained from equimolar solutions of commercially obtained potassium oxalate, oxalic acid and sulfuric acid at room temperature. 1% of VOSO₄ was added to the solution as a dopant. Well-developed single crystals were obtained within about a week. KTO possessed triclinic symmetry with space group $P\bar{1}$. The unit cell contained 2 formula units. Its dimensions were $a = 6.354 \text{ \AA}$, $b = 10.605 \text{ \AA}$, $c = 7.021 \text{ \AA}$, $\alpha = 86.13^\circ$, $\beta = 100.16^\circ$ and $\gamma = 78.10^\circ$ [27].

2.3. EPR Spectra

EPR spectra were recorded with a Varian E-109 X-band EPR spectrometer using 2 mW microwave power and a 1.2 G magnetic field modulation frequency of 100 kHz. The single crystal was glued on a quartz pillar of a goniometer graded in degrees and rotated at 5° or 10° intervals depending on the variation of the spectra in three mutually perpendicular planes. The powder spectra of the samples in a quartz tube were recorded. The spectrometer frequency was corrected using a DPPH (diphenylpicrylhydrazyl) sample ($g = 2.0036$). Simulations of powder spectra of both compounds were made using Bruker's WINEPR software.

2.4. Optical Absorption Spectra

The optical absorption spectra of VO²⁺ doped KDP and KTO single crystals were recorded at room temperature on a CINTRA 20 UV-VIS spectrometer having diffuse reflectance accessory working between 300 and 900 nm.

3. Results and Discussion

The single crystal EPR spectra of VO²⁺ doped KDP and KTO were taken at room temperature in three mutually perpendicular planes between 0° and 180°. Figure 1 shows the EPR spectrum of VO²⁺ doped KDP

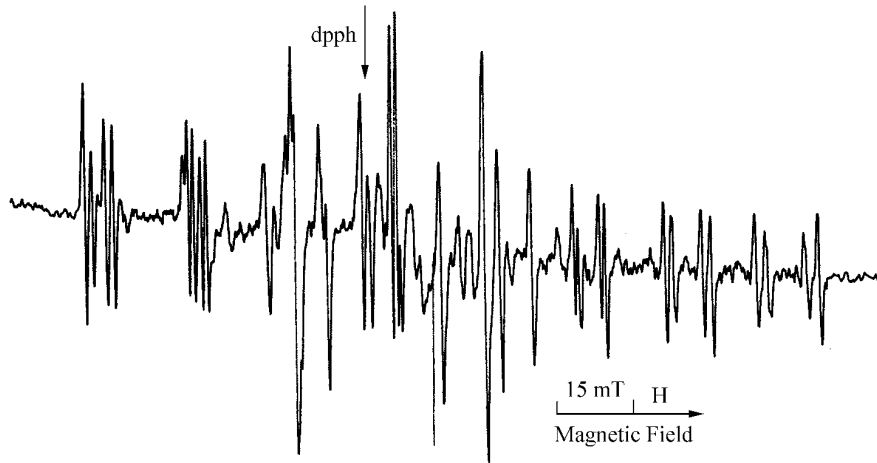


Fig. 2. EPR spectrum of VO²⁺ doped KDP single crystal with the magnetic field inclined by 170° relative to the *c* axis in the *bc* plane.

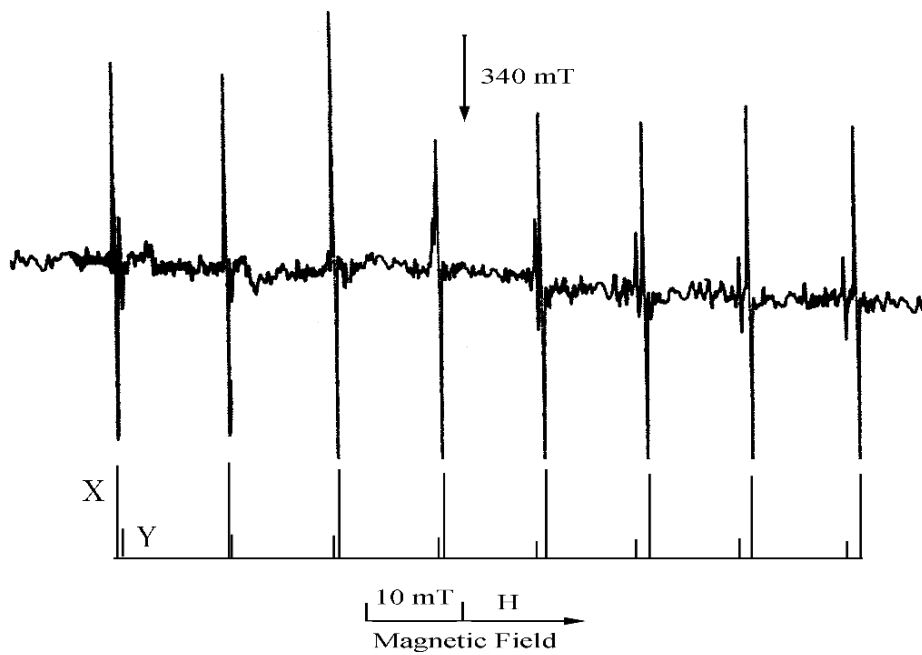


Fig. 3. EPR spectrum of VO²⁺ doped KTO single crystal with the magnetic field inclined by 130° relative to the *b* axis in the *a*b* plane.

single crystals in the *ca* plane with the magnetic field inclined by 5° to the *a* axis, and Fig. 2 shows the spectrum taken in the *bc* plane with the magnetic field inclined by 170° to the *c* axis. Figure 3 shows the spectrum of a KTO single crystal in the *a*b* plane with the magnetic field inclined by 130° to the *b* axis. The spectra arise from the paramagnetic VO²⁺ ion with the single d-electron interacting with the magnetic moment of the ⁵¹V nucleus (*I* = 7/2).

The plots of all detectable line positions (as *g*²) against the rotation angles for both samples are given in Figs. 4 and 5. *g*² of a line *k* as a function of the rota-

tion angle θ should be given by

$$g_k^2(\theta) = g_{ii}^2 \cos^2 \theta + g_{jj}^2 \sin^2 \theta + 2g_{ij}^2 \sin \theta \cos \theta, \quad (1)$$

where *i*, *j*, *k* = *x*, *y*, *z*, respectively, and θ is the angle of rotation in each crystalline plane with respect to the magnetic field direction. g_{ii}^2 , g_{jj}^2 and g_{ij}^2 are the **g** tensor elements, which will be found by fitting [28].

One can choose the points belonging to a specific line on the plots of Figs. 4 or 5 and fit them to (1). After determining all the lines on the plots, the detected lines belonging to a specific paramagnetic center are to be identified; that is the nuclear spin and *M_I* quantum val-

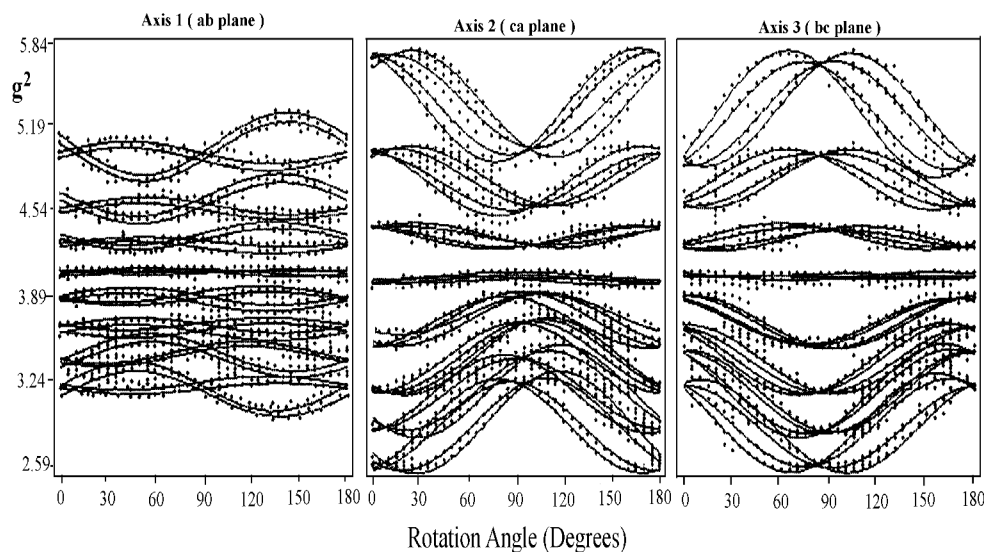


Fig. 4. Variation of the g^2 values of all lines in three planes of VO²⁺ doped KDP single crystal. The solid lines represent the least squares fitted values.

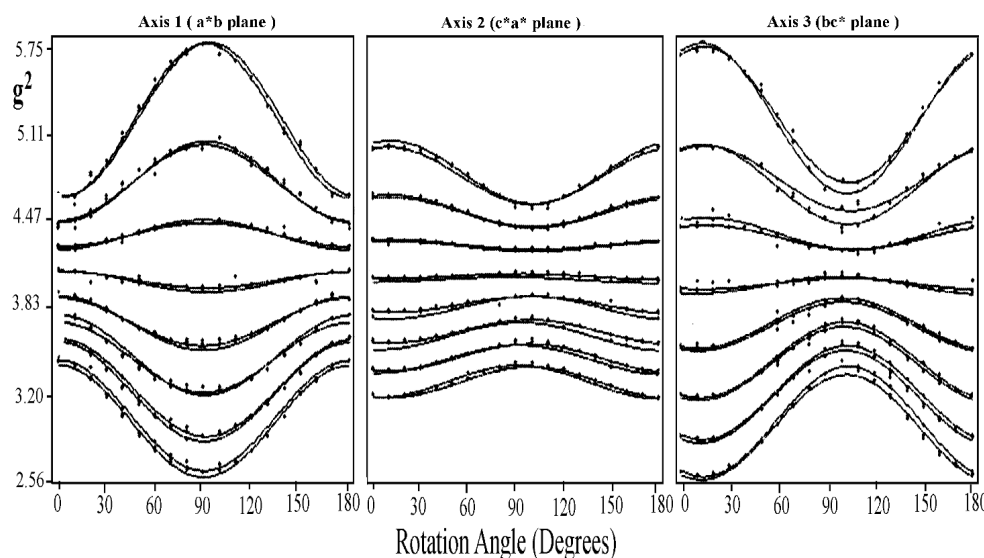


Fig. 5. Variation of the g^2 values of all lines in three planes of VO²⁺ doped KTO single crystal. The solid lines represent the least squares fitted values.

ues must be attributed to correct lines. And then the A and g values can be determined.

The EPR spectra of transition metal complexes are explained with the Hamiltonian including electron Zeeman, nuclear Zeeman and hyperfine coupling interactions:

$$\mathcal{H} = \beta \mathbf{H} \cdot \mathbf{g} \cdot \mathbf{S} + g_N \beta_N \mathbf{H} \cdot \mathbf{S} + \mathbf{I} \cdot \mathbf{A} \cdot \mathbf{S} \quad (2)$$

where \mathbf{g} and \mathbf{A} are the spectroscopic splitting and the hyperfine coupling tensors, respectively. Since the nuclear Zeeman interaction is small, it is neglected in most applications [3–5, 11].

A computer program, using an iterative algorithm, is used for the calculation of the \mathbf{g} and \mathbf{A} tensor elements from the detected and identified lines discussed above [29]. Each tensor is diagonalized and the principal values are obtained. The results are given in Table 1.

Figures 6 and 7 show the optical absorption spectra of VO²⁺ doped KDP and KTO single crystals. The optical absorption spectra show three absorption bands for both samples. The values are given in Table 2. The parallel components of the \mathbf{g} and \mathbf{A} tensors are not collinear due to the distortion of the [VO(H₂O)₅]²⁺ octahedra in the environments they stay in. The distor-

Complex	g_{\parallel}	g_{\perp}	A_{\parallel}	A_{\perp}	β_1^2	β_2^2	γ^2	κ	P
X ₁	1.923	1.998	19.39	7.61	0.975	0.904	0.395	0.809	137
X ₂	1.924	1.992	18.80	7.53	0.948	0.918	0.378	0.827	131
Y ₁	1.933	1.998	18.00	8.17	0.838	0.926	0.167	0.975	114
Y ₂	1.935	1.993	18.90	8.51	0.803	0.938	0.410	0.968	120
Powder									
X	1.925	1.997	19.06	7.24	0.940	0.919	0.307	0.784	137
Y	1.934	1.997	18.69	7.24	0.830	0.921	0.348	0.803	133
X	1.931	1.997	18.41	7.24	0.831	0.923	0.395	0.816	129
Y	1.938	1.994	18.58	6.85	0.735	0.943	0.302	0.761	136
Powder	1.929	1.995	19.01	7.46	0.856	0.920	0.273	0.812	134

Table 1. Principal g and hyperfine coupling tensor (A) values and calculated molecular orbital parameters of VO²⁺ complexes in KDP and KTO single crystals at room temperature ($\Delta g = \pm 0.005$, A and P are in units of 10^{-4} cm^{-1}).

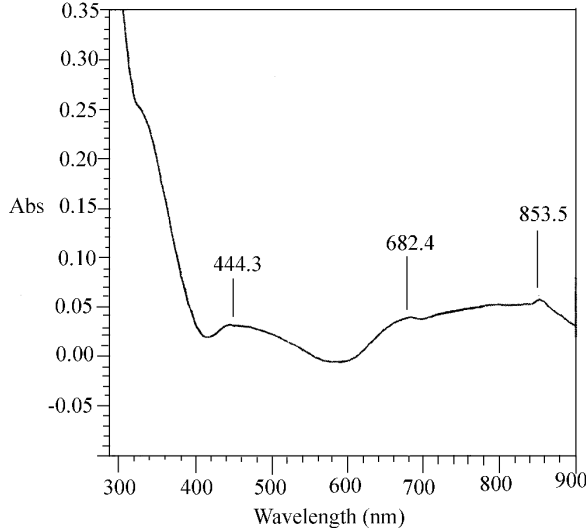


Fig. 6. Optical absorption spectrum of VO²⁺ doped KDP.

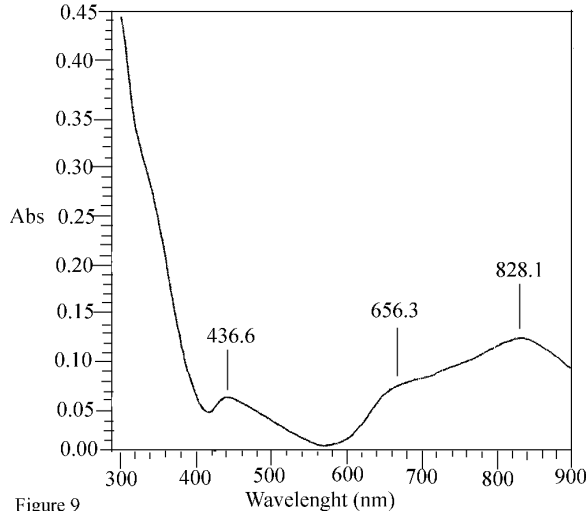


Figure 9

Fig. 7. Optical absorption spectrum of VO²⁺ doped KTO.

tion especially takes place along the V=O direction, and the degeneracy of the ground state of the vana-

Table 2. The optical absorption transition bands of VO²⁺ doped KDP and KTO complexes.

Transitions	Transition energy [cm^{-1}]	
	KTO	KDP
$\Delta_{\perp} = {}^2B_{2g} \rightarrow {}^2E_{2g}$	22904	22573
$\Delta_{\parallel} = {}^2B_{2g} \rightarrow {}^2B_{1g}$	15236	14654
$\Delta = {}^2B_{2g} \rightarrow {}^2A_{1g}$	12078	11716

dium atom in the 3d¹ configuration splits into $d_{x^2-y^2}$ and doubly degenerate d_{xz} and d_{yz} states [30, 31]. The molecular orbital coefficients can be calculated for vanadyl ions in both hosts by correlating the EPR and optical absorption data.

The molecular orbital parameters β_1^2 , β_2^2 and γ^2 , the Fermi contact term κ and the dipolar hyperfine coupling constant P can be calculated from the formulae [32–33]

$$g_{\parallel} = g_e \left(1 - \frac{4\lambda\beta_1^2\beta_2^2}{\Delta_{\parallel}} \right), \quad g_{\perp} = g_e \left(1 - \frac{\gamma^2\lambda\beta_2^2}{\Delta_{\perp}} \right) \quad (3)$$

and

$$A_{\parallel} = -P \left[\kappa + \frac{4}{7}\beta_2^2 + (g_e - g_{\parallel}) + \frac{3}{7}(g_e - g_{\perp}) \right], \quad (4)$$

$$A_{\perp} = -P \left[\kappa - \frac{2}{7}\beta_2^2 + \frac{11}{14}(g_e - g_{\perp}) \right].$$

β_1^2 and γ^2 are measures of the ionic degrees of σ and π bonds with equatorial ligands and are equal to unity if the bonds are purely ionic. For a completely ionic bond between vanadium and vanadyl oxygen, β_2^2 could also be unity [11, 34]. $g_e (= 2.0023)$ is the free electron g value and λ the spin orbit coupling constant of VO²⁺, which is known to be 170 cm^{-1} for the vanadium atom [9]. Δ_{\perp} and Δ_{\parallel} are energy separations from the ground state ${}^2B_{2g}$ to the two nearest higher states 2E_g and ${}^2B_{1g}$, respectively.

The molecular orbital parameters, Fermi contact term κ and dipolar hyperfine coupling constant P are

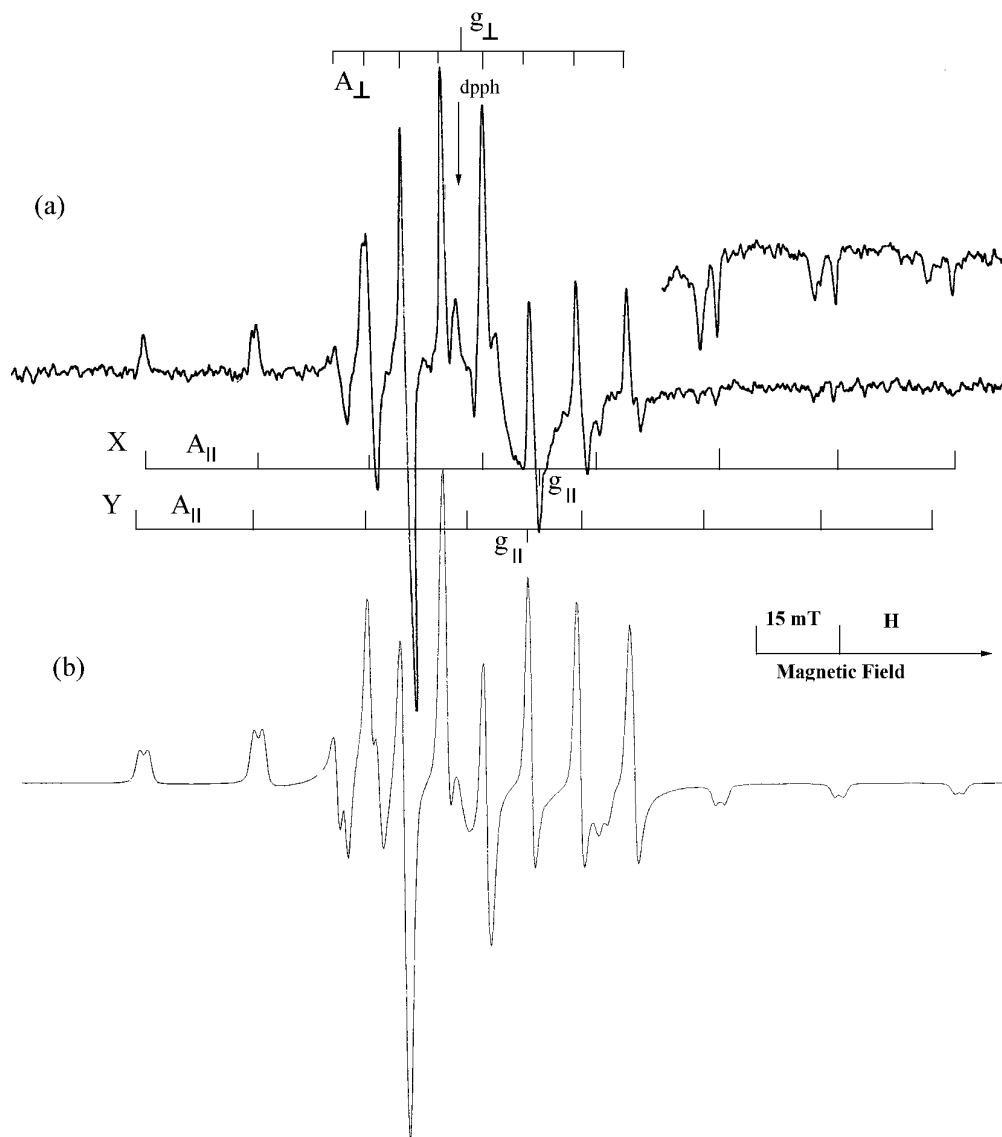


Fig. 8. Powder spectrum (a) and simulated spectrum (b) of VO²⁺ doped KDP.

calculated by ignoring second order effects [35]. These values are listed in Table 1.

3.1. VO²⁺ Doped KDP Single Crystal

The EPR spectra of a VO²⁺ doped KDP single crystal are taken in the three mutually perpendicular planes xy , zx and yz (which coincide with the ab , ca and bc planes of tetragonal axes, where $|a| = |b|$) for each 5°. Figures 1 and 2 show two sample spectra taken at different crystal orientations. In the spectrum shown in

Fig. 1 the lines of all sites superimpose onto a single vanadium spectrum. In Fig. 2, however, a large number of unidentifiable lines is seen. Since the lines overlap at almost all orientations and hence are untraceable, the identification and the precise resolution are made very carefully. If we consider the behavior of the spectra together with the plots of line positions in three planes, 32 lines can be identified and collected into four groups which belong to four VO²⁺ sites, as shown in Fig. 4 and given in Table 1. Tabulated values and the spectral behavior indicate that the observed four sites can be

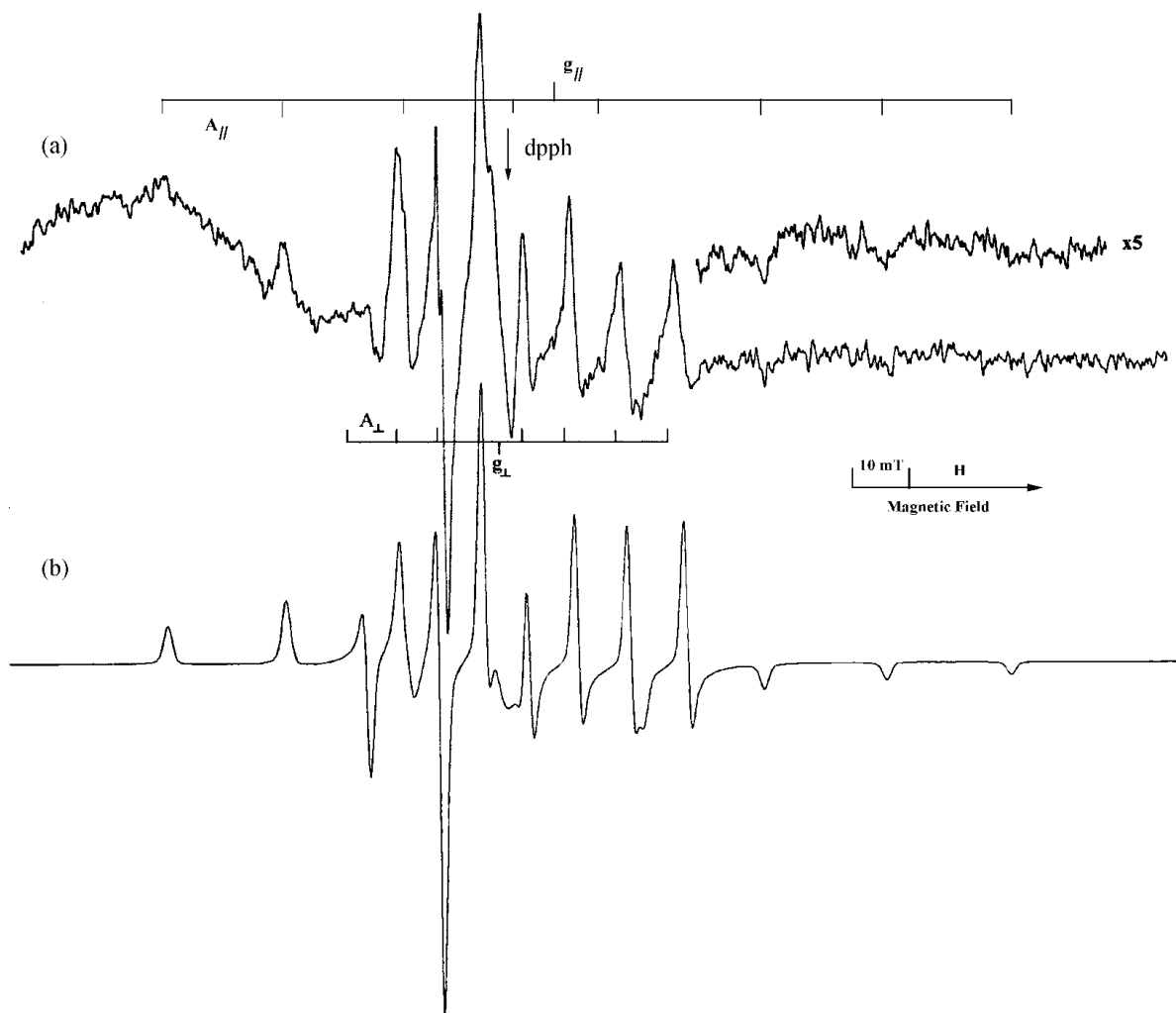


Fig. 9. Powder spectrum (a) and simulated spectrum (b) of VO²⁺ doped KTO.

divided into two groups X and Y. The principal g and hyperfine coupling values of sites X₁ and X₂, and those of sites Y₁ and Y₂ seem to be very close to each separately. Figure 8 shows the powder and simulated spectrum of VO²⁺ doped KDP. The values measured from the powder spectrum agree with the single crystal data. The simulation made using experimental values gives nearly the same spectrum. The differences in the parallel components of two groups are also observable in the powder spectrum. The perpendicular components of two groups, however, are not distinguished due to spectral overlap (see Table 1 and Fig. 8).

VO²⁺ ions substitute with K⁺ ions in the host by compensating the negative charge deficiency via oxygen atoms of PO₄³⁻ groups in the ligand positions.

The hydrogen splittings are not seen, indicating that the vanadyl ions are not close enough to those oxygen atoms which have bridging hydrogen atoms.

By correlating EPR and optical absorption data, spin Hamiltonian parameters and molecular orbital coefficients are calculated for the vanadyl ion and are given in Table 1. The degree of distortion can be estimated from Fermi contact terms κ and the P parameter. P is related to the radial distribution of the wave function of the ions and is defined as $P = g_e g_N \beta_e \beta_N \langle r^{-3} \rangle$. The parameter κ is sensitive enough to deformations of the electron orbitals of the central vanadium ion. The large value of κ indicates a large contribution to the hyperfine constant by the unpaired d electron in VO²⁺ and also probably a contribution from spin polariza-

tion [11]. For a free electron, the P value is $160 \cdot 10^{-4} \text{ cm}^{-1}$. The calculated value of P for KDP lies between $120 \cdot 10^{-4}$ and $137 \cdot 10^{-4} \text{ cm}^{-1}$, which indicates a considerable reduction from the free electron value. It is found by comparing the calculated and measured values of the P parameter, that the complex is fairly covalent in nature. There is no appreciable change in the P value when the vanadyl ion is surrounded by four water molecules and has a short V=O bond.

The β_2^2 values of all sites found in this work indicate explicitly that the bonds are nearly ionic, meaning that the π bonding to the ligands is rather weak. $1 - \beta_1^2$ and $1 - \gamma^2$ are considered as measures of covalency. In this work, γ^2 is found to be smaller than β_1^2 , meaning that in-plane σ bonding is more covalent than in-plane π bonding.

3.2. VO²⁺ Doped KTO Single Crystal

EPR spectra of single crystals of VO²⁺ doped KTO were measured for rotations in three mutually perpendicular planes. Figure 3 shows the EPR spectrum of VO²⁺ doped KTO single crystals with the magnetic field inclined by 130° from the a^* axis in the a^*b plane. As can be seen from the figure, there are two sets of octets arising from VO²⁺ ions with different intensities. The lines labeled as X are more intense than the

lines labeled as Y. The angular variations of the spectra in the three planes a^*b , c^*a^* and bc^* are shown in Figure 5. The lines are resolved, **A** and **g** tensors are constructed and principal values are calculated as discussed above. The results are given in Table 1. The existence of two spectral components seems at first sight to be incompatible with the triclinic symmetry. In fact the intense lines, labeled as X in the figure, arise from the ion where the oxalate groups are in ligand positions. The weak lines, labeled as Y, arise from an interstitial site with nearly the same structure and orientation. Principal **A** and **g** tensor elements show that both sites are nearly axially symmetric, as usual for most of the VO²⁺ complexes [3–10]. Figure 9 shows the powder and simulated spectrum of VO²⁺ doped KTO. The parallel and perpendicular components of the hyperfine and **g** coupling tensors are measured and given in Table 1 together with single crystal values. Vanadyl ions enter the lattice, substituting for K⁺ ions, and compensating the charge deficiency with nearby oxygen atoms. The C_4 axis of the octahedron coincides with the crystallographic b axis.

By correlating the EPR and optical absorption data, spin Hamiltonian parameters and molecular orbital coefficients are calculated, as discussed for the KDP crystal, and are given in Table 1. Similar evaluations made for KDP above are also valid for KTO.

- [1] D. P. Padiyan, C. Muthukrishnan, and R. Murugesan, *J. Mol. Struct.* **648**, 1 (2003).
- [2] N. O. Gopal, K. V. Narasimhulu, and J. L. Rao, *Physica B* **307**, 117 (2001).
- [3] B. Karabulut, İ. İlkin, and R. Tapramaz, *Z. Naturforsch.* **60a**, 95 (2005).
- [4] R. Tapramaz, B. Karabulut, and F. Köksal, *J. Phys. Chem. Solids* **61**, 1367 (2000).
- [5] R. Bıyık, R. Tapramaz, and B. Karabulut, *Z. Naturforsch.* **58a**, 499 (2003).
- [6] S. Radhakrishna and M. Sologram, *Solid State Commun.* **47**, 77 (1983).
- [7] V. K. Jain, *Phys. Status Solidi (b)* **97**, 337 (1980).
- [8] S. K. Misra and C. Wong, *Physica B* **159**, 321 (1989).
- [9] K. V. Narasimhulu and J. L. Rao, *Spectrochim. Acta A* **53**, 2605 (1997).
- [10] B. Karabulut and R. Tapramaz, *Z. Naturforsch.* **54a**, 370 (1999).
- [11] B. D. P. Raju, K. V. Narasimhulu, N. O. Gopal, and J. L. Rao, *J. Phys. Chem. Solids* **64**, 1339 (2003).
- [12] U. Straube and H. Bige, *J. Alloys Comp.* **310**, 181 (2000).
- [13] I. P. Kaminow, *Introduction to Electro-Optic Devices*, Academic Press, New York 1974.
- [14] F. Zernike and J. E. Midwinter, *Applied Nonlinear Optics*, John Wiley and Sons, New York 1973.
- [15] For large KDP crystals growing and applications visit <http://clevelandcrystals.com>.
- [16] H. Koga and K. Hukuda, *J. Phys. Soc. Jpn.* **25**, 630 (1968).
- [17] A. Otani and S. Makhisima, *J. Phys. Soc. Jpn.* **26**, 85 (1969).
- [18] T. A. Eremina, N. N. Eremin, V. A. Kuznetsov, T. M. Okhrimenko, N. G. Furmanova, E. P. Efremova, and V. S. Urusov, *Crystallography Rep.* **47**, Suppl. 1, 76 (2002).
- [19] N. Y. Garces, K. T. Stevens, L. E. Halliburton, M. Yan, N. P. Zaitseva, and J. J. DeYoreo, *J. Cryst. Growth* **225**, 435 (2001).
- [20] J. Podder, *J. Cryst. Growth* **237**, 70 (2002).
- [21] S. Seif, K. Bhat, A. K. Bata, M. D. Aggarwal, and R. B. Lal, *Mater. Lett.* **58**, 991 (2004).
- [22] N. Y. Garces, K. T. Stevens, L. E. Halliburton, S. G. Demos, H. B. Radousky, and N. P. Zaitseva, *J. Appl. Phys.* **84**, 47 (2001).

- [23] S. Hirota, H. Miki, K. Fukui, and K. Maeda, *J. Cryst. Growth* **235**, 541 (2002).
- [24] Y. Wong and E. J. Reardon, *Appl. Geochem.* **16**, 531 (2001).
- [25] R. P. Buck, S. Rondinini, A. K. Covington, F. G. K. Baucke, C. M. A. Brett, M. F. Camoes, M. J. T. Milton, T. Mussini, R. Naumann, K. W. Pratt, P. Spitzer, and G. S. Wilson, *Pure Appl. Chem.* **74**, 2169 (2002).
- [26] J. Oakes and M. C. Caf e, *Eur. J. Biochem.* **36**, 559 (1973).
- [27] M. Curie and J. C. Speakman, *J. Chem. Soc. A*, 1862 (1967).
- [28] N. M. Atherton, *Electron Spin Resonance Theory and Applications*, John Wiley and Sons, New York 1973.
- [29] B. Karabulut and R. Tapramaz, *Radiat. Chem. Phys.* **55**, 331 (1999).
- [30] M. Narayana, G. Sathyanarayan, and G. S. Sastry, *Mol. Phys.* **31**, 96 (1997).
- [31] T. F. Yen, L. J. Boucher, and E. C. Tynan, *Electron Spin Resonance of Metal Complexes*, Plenum, New York 1969.
- [32] C. R. Ballhausen and B. G. Gray, *Inorg. Chem.* **1**, 111 (1961).
- [33] D. Kivelson and S. K. Lee, *J. Chem. Phys.* **41**, 1896 (1964).
- [34] A. Murali, J. L. Rao, and A. V. Subbaiah, *J. Alloys Comp.* **257**, 96 (1997).
- [35] L. J. Boucher, E. C. Ynan, and T. F. Yen, *Electron Spin Resonance of Metal Complexes*, Plenum, New York 1969.